

Full length article

## Bulk tracer diffusion in CoCrFeNi and CoCrFeMnNi high entropy alloys

M. Vaidya <sup>a, b, \*</sup>, K.G. Pradeep <sup>c</sup>, B.S. Murty <sup>b</sup>, G. Wilde <sup>a, d</sup>, S.V. Divinski <sup>a, e, \*\*</sup><sup>a</sup> Institute of Materials Physics, University of Münster, Wilhelm-Klemm-Str. 10, 48149, Münster, Germany<sup>b</sup> Department of Metallurgical & Materials Engineering, Indian Institute of Technology Madras, Chennai, 600036, India<sup>c</sup> Materials Chemistry, RWTH Aachen University, Kopernikusstr. 10, 52074, Aachen, Germany<sup>d</sup> Herbert Gleiter Institute of Nanoscience, Nanjing University of Science and Technology, 200 Xiaolingwei Avenue, Nanjing, 210094, China<sup>e</sup> Samara National Research University, Moskovskoye Shosse 34, Samara, 443086, Russia

## ARTICLE INFO

## Article history:

Received 21 October 2017

Received in revised form

10 December 2017

Accepted 23 December 2017

Available online 11 January 2018

## Keywords:

High entropy alloys

Diffusion

Activation energy

Compensation effect

## ABSTRACT

High entropy alloys (HEAs) have emerged as a promising class of equiatomic or near equiatomic multicomponent alloys, which garner fundamental curiosities and interest in high temperature applications. Understanding diffusion kinetics of HEAs is critical to assess their phase stability and deformation behaviour, particularly at elevated temperatures. For the first time, bulk tracer diffusion coefficients of Co, Cr, Fe and Mn are determined in polycrystalline CoCrFeNi and CoCrFeMnNi HEAs using the radiotracer method in the temperature interval of 1073–1373 K. Material homogeneity and the absence of any phase decomposition in CoCrFeNi and CoCrFeMnNi HEAs were established by electron microscopy and atom probe tomography investigations.

Both bulk and grain boundary diffusion contributions to penetration profiles are observed for diffusion of Co, Cr, Fe and Mn tracers in both HEAs. The temperature dependencies of bulk diffusion for all tracers show Arrhenius behaviour. The corresponding activation energies ( $Q$ ) and the logarithm of pre-exponential factors ( $D_0$ ) show a linear relationship, thus following the “compensation rule”. An increase of the configurational entropy leads to reduced diffusion rates only when a homologous temperature scale is used for comparison. The increase of activation energy barrier and lower frequency factors both contribute to the decreased diffusion rates. A cross-over temperature ( $T_c = 1020$  K) is observed for Co diffusion (on slight extrapolation of Arrhenius plot) in CoCrFeNi and CoCrFeMnNi HEAs, while Cr and Fe exhibit almost parallel Arrhenius lines. Above  $T_c$ , the Co diffusivity is higher in CoCrFeMnNi than in CoCrFeNi, which suggests that diffusion in HEAs need not be assumed to retard with an increasing number of elements. The existence of a cross-over temperature correlates with the change in binding energy (or enthalpy) of the constituents from CoCrFeNi to CoCrFeMnNi.

© 2018 Acta Materialia Inc. Published by Elsevier Ltd. All rights reserved.

## 1. Introduction

Materials development has always been at the forefront of technological advancements. A majority of alloy development until now has been done following the conventional strategy of choosing a base element and making suitable additions to it to achieve desired properties. A new class of multicomponent alloys termed as high entropy alloys (HEAs) have evolved over the last decade,

which contain equiatomic or near-equiatomic proportion of elements [1]. Thus, their lattice can be regarded as a no-solvent or whole-solute matrix. These multicomponent alloys often show simple solid solution structures presumably stabilized by their high configurational entropy of mixing ( $\Delta S_{\text{mix}}$ ) [2]. HEAs have revealed promising properties such as high strength combined with ductility [3], high fracture toughness [4], excellent oxidation [5] and corrosion resistance [6] that generate interest for technological applications. HEAs have also spawned fundamental curiosities like phase diagrams for multicomponent systems, atomic occupancies in a complex lattice and diffusion in a multiprincipal element matrix [7]. Understanding diffusion kinetics is critical to assess the phase stability and deformation characteristics of HEAs, which are key parameters to evaluate the performance of any novel material. However, investigations of the diffusion behaviour of HEAs have

\* Corresponding author. Institute of Materials Physics, University of Münster, Wilhelm-Klemm-Str. 10, 48149, Münster, Germany.

\*\* Corresponding author. Institute of Materials Physics, University of Münster, Wilhelm-Klemm-Str. 10, 48149, Münster, Germany.

E-mail addresses: [mm12d022@smail.iitmadras.ac.in](mailto:mm12d022@smail.iitmadras.ac.in) (M. Vaidya), [divin@www.de](mailto:divin@www.de) (S.V. Divinski).

been scarce and largely limited to the application of an interdiffusion (couple) technique. Table 1 enlists all the literature reports available so far, to the best of our knowledge, in a chronological order, on diffusion in HEAs along with the alloy studied, methodology adopted and important conclusions derived.

The interdiffusion measurements utilizing a diffusion couple technique seem to confirm the original paradigm of sluggish diffusion in HEAs [8,9,11], while the only available direct tracer diffusion results hint towards a non-sluggish atomic transport [12,15]. There is lack of consensus yet on the factors responsible for the anticipated decelerated diffusivities. Increased activation barriers [8], correlation effects [9,10], a combination of energy and entropic terms [12] and crystallographic structure [16] have been found to influence the diffusion rates in HEAs. In addition, the diffusion kinetics of only three HEA systems have been analyzed so far. Despite the vast compositional space of HEAs, true single phase HEAs are very few [7], which makes reliable diffusion measurements difficult.

In our recent work [12], Ni tracer diffusion in polycrystalline CoCrFeNi and CoCrFeMnNi HEAs was measured for the first time using the radiotracer technique, which is the most direct and reliable technique for bulk diffusion measurements. Two contributions to the concentration profiles were unambiguously observed and they were identified as bulk and grain boundary diffusion paths. A detailed analysis of bulk tracer diffusion of Ni showed a certain deceleration of the diffusion rates in HEAs compared to those in pure metals, binary or ternary alloys only when the diffusion rates were compared at the same homologous temperatures,  $T/T_m$  ( $T_m$  is the melting point of the corresponding compound). A comparison at a given absolute temperature  $T$  substantiates an increase of the Ni diffusion rate with an increase of the number of principal

elements when going from CoCrFeNi to CoCrFeMnNi alloy. In addition, a cross-over temperature was observed for Ni diffusion in HEAs, above which CoCrFeMnNi exhibited higher Ni diffusivity than CoCrFeNi. Thus it was concluded that diffusion in HEAs cannot be a-priori considered as sluggish and configurational entropy is not alone responsible for the reduced diffusion rates if the homologous temperature scale is used for comparison.

The obvious question that arises is whether this behaviour holds true for bulk diffusion of other elements or not? In this work, the bulk tracer diffusivities of all the remaining constituents (Co, Cr, Fe and Mn) in CoCrFeNi and CoCrFeMnNi HEAs are measured using the radiotracer technique. The inferences drawn are critically compared to the conclusions derived from the Ni tracer diffusion results in Ref. [12] and the premise of sluggish diffusion in HEAs is analyzed.

## 2. Experimental details

Metal pieces (99.9% pure) of Co, Cr, Fe, Mn and Ni were added together in equiatomic proportions to produce CoCrFeNi and CoCrFeMnNi HEAs by vacuum arc melting followed by homogenization at 1473 K for 50 h. The details of alloy preparation and structural characterization using both X-ray diffraction (XRD) and scanning electron microscopy (SEM) equipped with electron backscatter diffraction (EBSD) are given in Ref. [12]. Local electrode atom probe tomography (LEAP 4000X HR) provided by CAMECA instruments was used to investigate the absence of atomic scale phase separation or decomposition. A FEI Helios Nanolab 660 dual beam focussed ion beam has been employed to prepare atom probe tips following the procedures described in Refs. [17,18]. The atom probe tomography (APT) measurements were performed with the

**Table 1**  
Investigations on diffusion in high entropy alloys available so far in literature.

Alloy	Exp/Theor	Technique/Methodology used	Important results and conclusions	Ref.
CoCrFeMnNi	Exp	Interdiffusion experiment using quasi-binary approach and estimates of tracer diffusion coefficients	1. Sluggish diffusivities in HEAs 2. Intrinsic diffusion coefficients derived can be taken as tracer diffusion coefficients 3. Higher normalized activation energy of diffusion in HEAs	[8]
Co-Cr-Fe-Ni	Exp	Interdiffusion experiment with Dayanand-Sohn analysis	Diffusional interactions cannot be ignored while describing diffusion in HEAs	[9]
CoCrFeMnNi	Theor	Analysis of interdiffusion results presented in Ref. [8] using semi-empirical rules	1. Sluggish diffusion character of HEAs 2. Correlation effects play more important role than activation energies in slow diffusion	[10]
Al-Co-Cr-Fe-Ni	Exp	Interdiffusion experiment with Darken manning formalism for analysis	1. Sluggish diffusion in HEAs 2. Crystallographic structure has larger effect on diffusion coefficients than varied chemical environments by complex HEA matrix	[16]
CoCrFeNi and CoCrFeMnNi	Exp	Radiotracer method to determine Ni bulk diffusivity in HEAs	1. Both frequency factor and activation energy are important for diffusion in HEAs 2. Diffusion in HEAs should not be assumed as "sluggish"	[12]
CoCrFeMn <sub>0.5</sub> Ni	Theor	Analysis of interdiffusion results for multicomponent alloys by MAA <sup>b</sup> light approach, with application to experimental results presented in Ref. [8]	1. Correlation effects are highest for fastest diffusing species (Mn in CoCrFeNiMn) and do not affect the slowest moving element (Ni) 2. Correlation effects alone are not sufficient to explain sluggish diffusion of all components in HEAs	[13]
CoCrFeMn <sub>0.5</sub> Ni	Theor	Analysis of interdiffusion results presented in Ref. [8] by three random alloy approaches – Darken, combined Manning and HE <sup>a</sup> and MAA <sup>b</sup> light approaches	1. Results from random alloy solutions in good agreement with the experimental results 2. Very similar self-diffusion coefficients for all components	[14]
CoCrFeNi and CoCrFeMnNi	Exp	Radiotracer method to determine Ni grain boundary diffusivity in HEAs	Non-sluggish nature of GB diffusion in HEAs	[15]

<sup>a</sup> Holdsworth and Elliott.

<sup>b</sup> Moleko, Allnatt and Allnatt.

tips maintained at 60 K applying laser pulses at 250 kHz frequency and 20 pJ laser pulse energy. The IVAS 3.6.10 software has been used for data reconstruction and analysis.

The radioactive isotopes used as tracers for diffusion measurements in this work are:

<sup>57</sup>Co: half-life of 271.7 days, 122 keV  $\gamma$  decays

<sup>51</sup>Cr: half-life of 27.7 days, 320 keV  $\gamma$  decays

<sup>54</sup>Mn: half-life of 312 days, 834 keV  $\gamma$  decays

<sup>59</sup>Fe: half-life of 44.6 days, 1095 keV,  $\gamma$  decays

A highly diluted acidic solution of these isotopes was deposited on the surface of disc-shaped (8 mm diameter and 1 mm thickness) samples and left for drying. This was preceded by mechanical polishing of the samples to achieve a mirror-like finish. Subsequently, the samples were sealed in quartz tubes under purified (5N) Ar atmosphere and subjected to diffusion annealing treatments in the temperature range 1073–1373 K. The furnace temperature was controlled within  $\pm 1$  K with the aid of a Ni/NiCr thermocouple (type K). After annealing, the sample diameter was reduced by 1 mm to eliminate errors caused by surface or lateral diffusion. A serial sectioning technique, using a high-precision grinding machine, was used to determine the penetration profiles. Thickness reduction accuracy up to 0.05  $\mu\text{m}$  could be achieved. The intensity of  $\gamma$ -decays was determined by a solid Ge- detector equipped with a multi-channel energy discriminator and the counting times were chosen such that the statistical uncertainty of the measurements was less than 2% in all relevant energy windows. The usage of the multi-channel energy discriminator allowed simultaneous and reliable determination of the concentration profiles for all four isotopes in a single diffusion experiment.

### 3. Results

#### 3.1. Microstructure and chemical homogeneity of alloys

XRD and SEM results presented in Ref. [12] revealed that the CoCrFeNi and CoCrFeMnNi HEAs crystallize in the FCC structure, with equiatomic composition and uniform distribution of elements. The grain size of both the alloys was found to be in excess of 250  $\mu\text{m}$ . Using differential thermal analysis (DTA), the melting points of the alloys,  $T_m$ , were determined to be 1717 K and 1607 K for CoCrFeNi and CoCrFeMnNi respectively [12]. It may be noted that the “ $T_m$ ” corresponds to the peak temperatures of the melting transitions observed in DTA traces for the respective alloys. The difference between the liquidus and solidus is extremely small for both the alloys.

The coarse grain size and single phase microstructure of homogenised alloys is further confirmed by EBSD phase maps of CoCrFeNi and CoCrFeMnNi, see Fig. 1a and b, respectively. To validate the homogeneity in the local chemical composition and elemental distribution of the HEAs studied, APT investigations have been carried out for the CoCrFeNi and CoCrFeMnNi alloys. The spatial 3D arrangement of all the constituent elements for the CoCrFeNi and CoCrFeMnNi alloys along with their binomial frequency distribution is presented Figs. 2 and 3, respectively. It can be observed that all the elements are homogeneously distributed within the analyzed volume. The binomial frequency analysis further confirms a random distribution of all the elements without any phase separation. The degree of randomness is measured by the parameter  $\mu$  which varies between 0 and 1, where 0 stands for a complete randomness and 1 indicates clustering or precipitations [19,20]. As can be seen in Figs. 2 and 3, the experimentally obtained frequency distribution for all the constituent elements is in good agreement with their corresponding theoretical binomial

distribution of a random solid solution. In addition to the constituent elements, trace amount (<0.05 at.%) of impurity C was detected which as well shows homogeneous and random distribution.

#### 3.2. Co diffusion in HEAs

The geometry of the present experiments corresponds to tracer diffusion into semi-infinite sample. This initial situation refers mostly to the instantaneous source fulfilling the conditions of a thin film geometry [21], for which the Gaussian solution of the bulk diffusion equation is applicable,

$$C(x, t) = \frac{M}{\sqrt{\pi Dt}} \exp\left(-\frac{x^2}{4Dt}\right) \quad (1)$$

Here  $C(x, t)$  is the concentration at the depth  $x$  from the surface after the time  $t$ ,  $D$  is the diffusion coefficient, and  $M$  is the initial tracer amount. The complementary error function solution [21] was found to be more appropriate in some cases, especially at lower temperatures.

A distinct grain boundary contribution to the penetration profile under the present conditions corresponds to the B-type kinetic regime after Harrison's classification [22], which can be analyzed using Le Clair's functional form [23],

$$C(x, t) = C_0 \exp\left(-A \cdot x^{6/5}\right) \quad (2)$$

where  $C_0$  and  $A$  are constants.

The <sup>57</sup>Co concentration profiles measured at 1173 K for CoCrFeNi and CoCrFeMnNi are given in Fig. 4a and b, respectively. A combination of Eqs. (1) and (2) has been used to fit the experimental data and the  $R^2$  values larger than 0.9 have been obtained in each case. Thus, it is evident that both bulk and grain boundary diffusion contribute to the penetration profiles obtained. The first, near-surface branch of the profile corresponds to a bulk tracer diffusion mechanism. Both the alloys have a very large grain size,  $d$  (> 250  $\mu\text{m}$ ), consequently the ratio of the grain boundary width ( $\delta$ ) to  $d$  is very small, which further substantiates that only lattice diffusion is dominant in the regions close to the surface [21]. It has been conclusively shown in our previous results on Ni bulk and grain boundary diffusion that the second branch in such a penetration profile certainly corresponds to grain boundary diffusion [12,15].

The diffusion data from the first branch of the concentration profiles has been extracted and plotted against the penetration depth squared, as illustrated for Co diffusion in CoCrFeMnNi (Fig. 5). The maximum penetration depth increases with increasing temperature and the diffusion coefficient,  $D$ , is determined as

$D = -\left(\frac{1}{4t}\right) \cdot \left(\frac{\partial \ln C}{\partial x^2}\right)^{-1}$ , where  $\frac{\partial \ln C}{\partial x^2}$  is the slope of the penetration profile in the corresponding coordinates, cf. Eq. (1). The estimated uncertainty of the determined tracer diffusion coefficients in a typical measurement is below 20%.

For a given crystal structure, the diffusivities often scale with the corresponding melting points of the materials,  $T_m$ , [24]. The diffusion coefficients determined from concentration profiles are therefore plotted as functions of the inverse temperature,  $T^{-1}$ , and of the inverse homologous temperature,  $T_m/T$ , in Fig. 6 for Co diffusion in both HEAs. When compared against the homologous temperature, Co exhibits a lower diffusivity in CoCrFeMnNi than CoCrFeNi (Fig. 6a). The trend, however, is reversed when the diffusion rates are assessed on the absolute temperature scale (Fig. 6b). A cross-over temperature ( $T_c$ ) is also observed above which the diffusion rate of Co in CoCrFeMnNi is higher than in

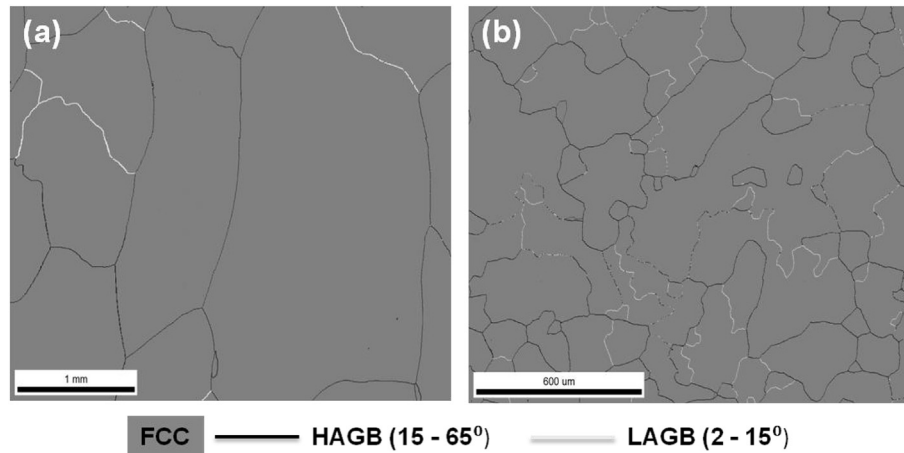


**Fig. 1.** EBSD phase maps for a) CoCrFeNi and b) CoCrFeMnNi alloys. A single phase FCC is indexed and different types of GBs are shown with different grey level lines. Coarse grain structure with predominantly high angle grain boundaries (HAGBs) is observed.

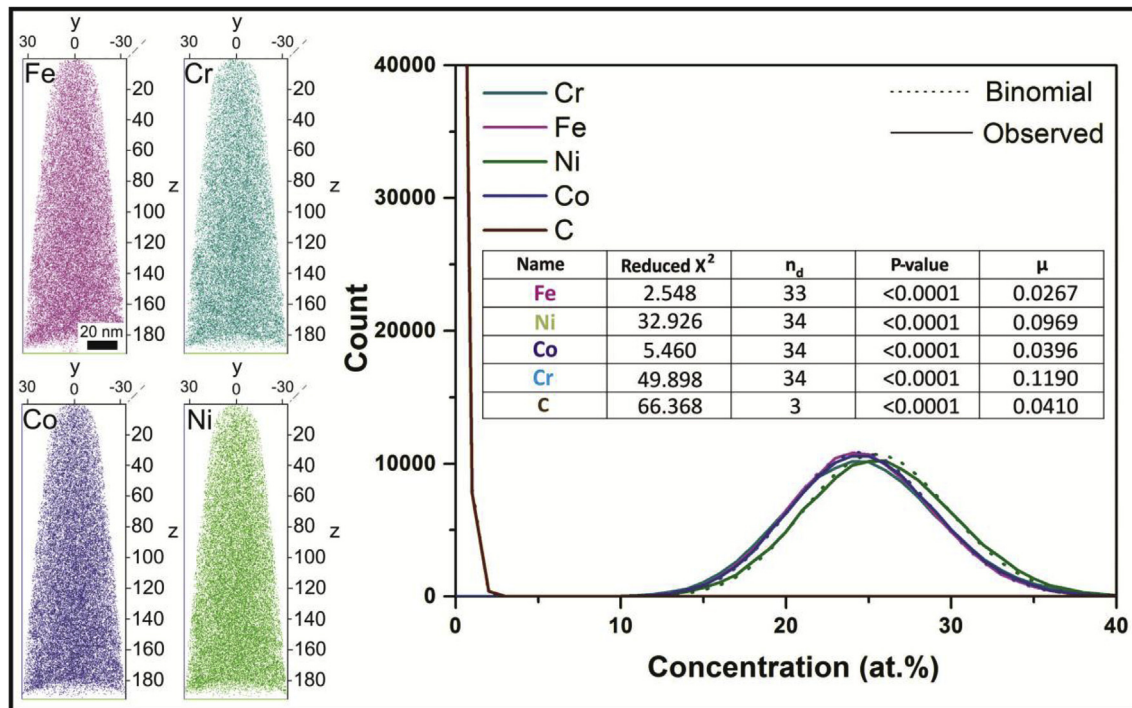


**Fig. 2.** Three dimensional reconstruction of the individual atomic positions for all the constituent elements in an analyzed volume of  $67 \times 67 \times 190 \text{ nm}^3$  and the corresponding binomial frequency distribution analysis with 100 ions per bin to verify homogeneity in CoCrFeNi HEA.

CoCrFeNi. The value of  $T_c$  for Co diffusion is 1020 K. It may be noted that the value of  $T_c$  is obtained after extrapolating the Arrhenius lines of diffusion in both HEAs to lower temperatures (or higher  $1/T$ ). This is a reasonable supposition as the microstructure of these HEAs is thermally stable upto the melting point [12] and thus the mechanism of diffusion does not change allowing  $Q$  to be assumed constant even outside the actual temperature range of diffusion measurements.

### 3.3. Cr and Fe bulk diffusion in HEAs

Both Cr and Fe crystallize in the BCC structure at room temperature and the investigation of their diffusion behaviour in a complex FCC matrix of HEAs is particularly interesting. Fig. 7a and b

exemplify the diffusion profiles of Cr in CoCrFeNi and CoCrFeMnNi HEAs at 1223 K. The grain boundary contribution to the measured penetration profiles of Cr is relatively less pronounced compared to the corresponding Co diffusion profiles at 1173 K (Fig. 5). This indicates lower values of the corresponding Le Clair parameter  $\beta$  for Cr (for details see Ref. [17]). Bulk and grain boundary diffusion contributions are clearly observed in the concentration profiles of Fe diffusion in CoCrFeNi (Fig. 8a) and CoCrFeMnNi (Fig. 8b) too. The bulk diffusion coefficients of Cr and Fe are determined at all temperatures by fitting the experimental data to equations (1) or (2). The radioactive isotopes of both Cr and Fe have short half-lives (27.8 and 44.6 days, respectively) and the diffusion coefficients were determined including the necessary corrections for isotope half-life.

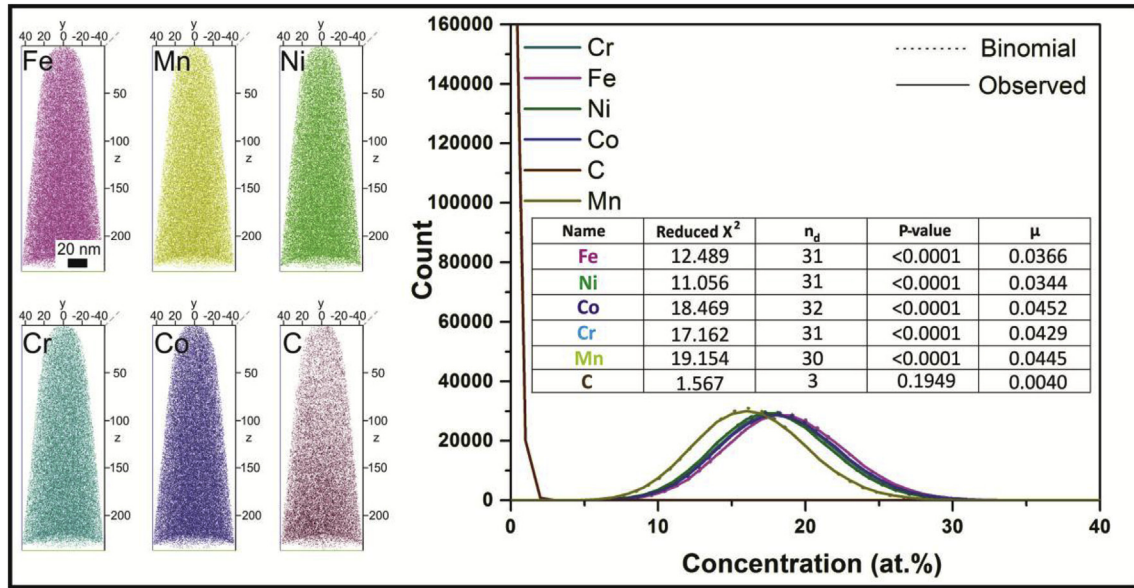


Fig. 3. Three dimensional reconstruction of the individual atomic positions for all the constituent elements in an analyzed volume of  $90 \times 90 \times 230 \text{ nm}^3$  and the corresponding binomial frequency distribution analysis with 100 ions per bin to verify homogeneity in CoCrFeMnNi HEA.

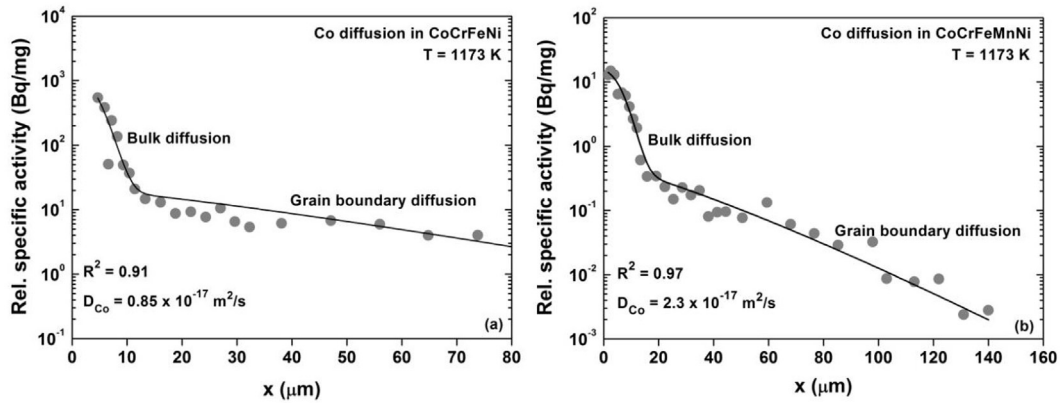


Fig. 4. Concentration profiles of Co tracer diffusion measured at 1173 K in (a) CoCrFeNi and (b) CoCrFeMnNi alloys. The solid lines represent fits according to simultaneous bulk and grain boundary diffusion.

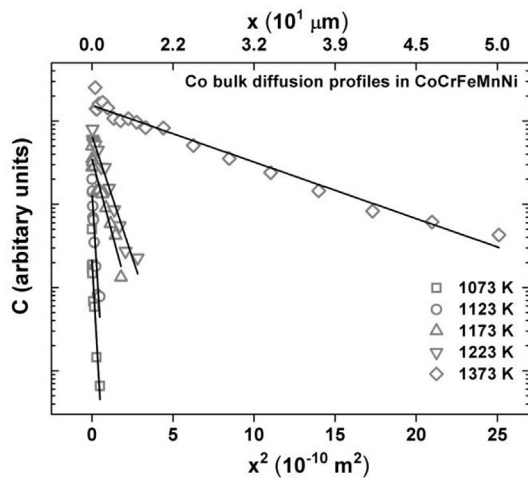


Fig. 5. The first branches (bulk diffusion) of the concentration profiles measured for Cr diffusion in CoCrFeMnNi.

Fig. 9a and b presents the first branches of the penetration profiles plotted against  $x^2$  for Cr and Fe diffusion in CoCrFeMnNi. The adequate fits and increasing penetration depths with temperature substantiate further the presence of bulk diffusion in the near-surface regions.

Fig. 10a shows the Cr diffusion coefficients in CoCrFeNi and CoCrFeMnNi plotted against the inverse homologous temperature. A nearly constant (temperature independent) decrease of the diffusion rates by, approximately, an order of magnitude can be seen for the quinary alloy relative to the quaternary one. The comparison of Cr diffusivities on the absolute temperature scale (Fig. 10b) reveals a slightly higher atomic transport rate in CoCrFeMnNi. Unlike Co, no cross-over temperature is seen for Cr diffusion in HEAs.

The temperature dependence of Fe bulk diffusion in HEAs reveals a similar behaviour to Cr. Diffusion of Fe in CoCrFeMnNi proceeds with lower rates than in CoCrFeNi when examined using the homologous temperature scale (Fig. 11a). The Fe diffusion rates are similar in CoCrFeNi and CoCrFeMnNi when assessed on the  $1/T$  scale (Fig. 11b). A cross-over temperature is not observed for Fe

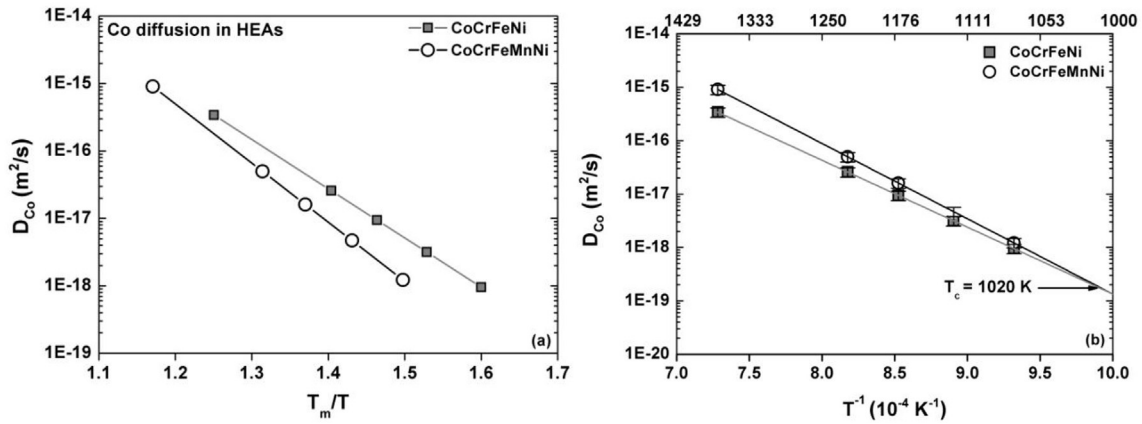


Fig. 6. Arrhenius diagrams for Co diffusion in CoCrFeNi and CoCrFeMnNi alloys plotted using (a) the inverse homologous temperature or (b) the inverse absolute temperature.

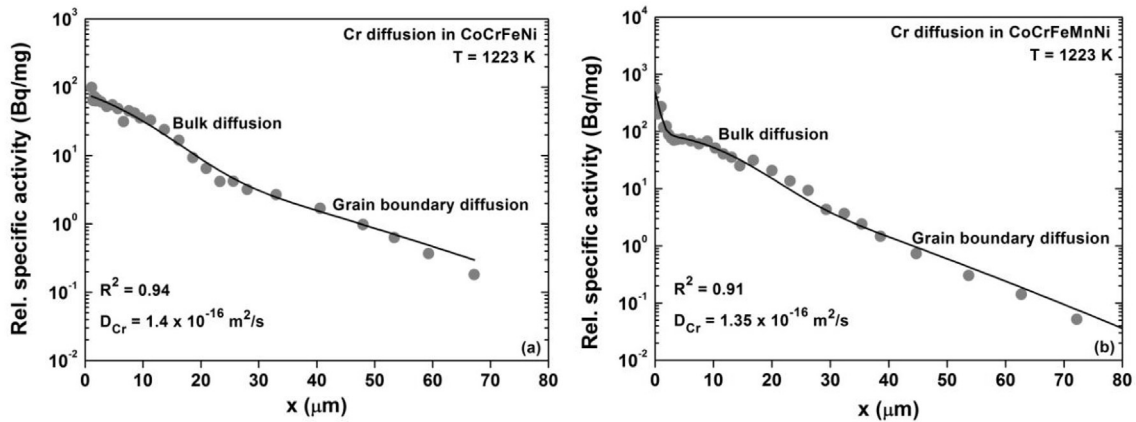


Fig. 7. Concentration profiles of Cr tracer diffusion measured at 1173 K in (a) CoCrFeNi and (b) CoCrFeMnNi alloys. A faster rate of GB diffusion is indicated.

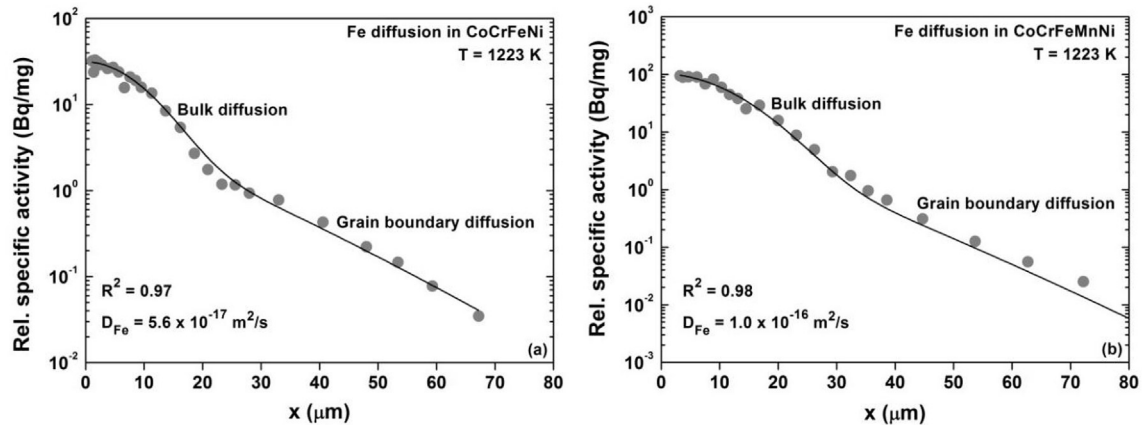


Fig. 8. Concentration profiles of Fe tracer diffusion measured at 1173 K in (a) CoCrFeNi and (b) CoCrFeMnNi alloys.

diffusion in HEAs as well.

### 3.4. Mn bulk diffusion in HEAs

Mn is the element with the lowest melting point among the constituents of the CoCrFeMnNi alloy and exhibits a complex cubic structure. Like other tracers, the penetration profile for Mn diffusion in polycrystalline CoCrFeMnNi shows two branches

corresponding to bulk and grain boundary diffusion (Fig. 12a). As pointed out earlier, a typical uncertainty of the diffusion coefficient measurements using the radiotracer method is below 20% when similar experimental conditions are maintained. Mn has the highest vapour pressure among all elemental components of CoCrFeMnNi and therefore will be most prone to errors or uncertainties in the diffusivity measurements. Hence, the Mn diffusion measurements were repeated at 1173 K for shorter (16 h) and longer

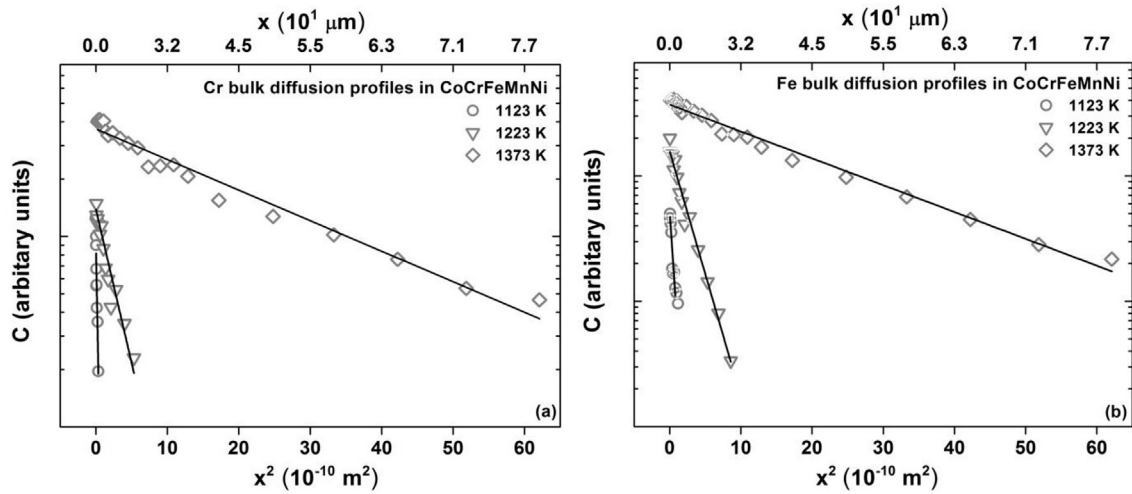


Fig. 9. The first branches (bulk diffusion) of the concentration profiles measured for a) Cr and b) Fe diffusion in CoCrFeMnNi.

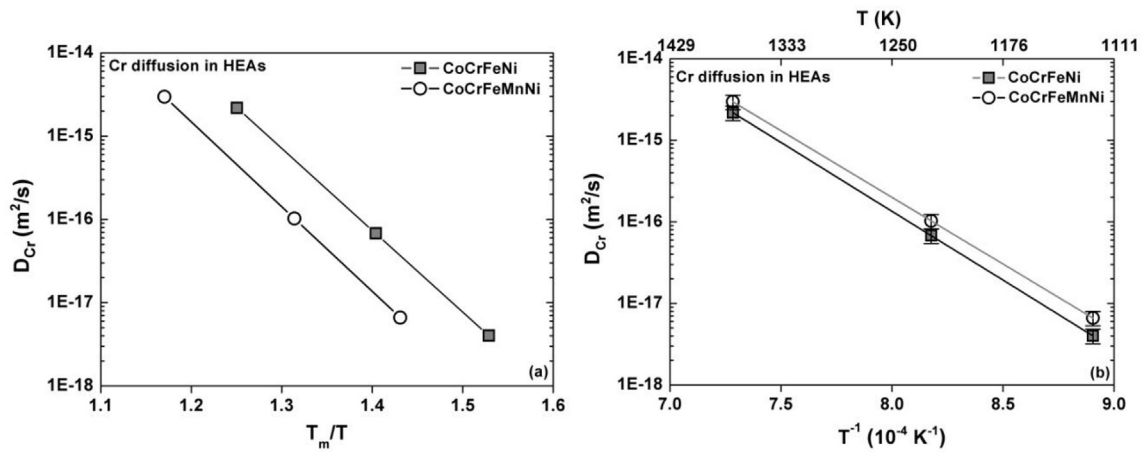


Fig. 10. Arrhenius diagrams for Cr diffusion in CoCrFeNi and CoCrFeMnNi alloys plotted using (a) the inverse homologous temperature or (b) the inverse absolute temperature.

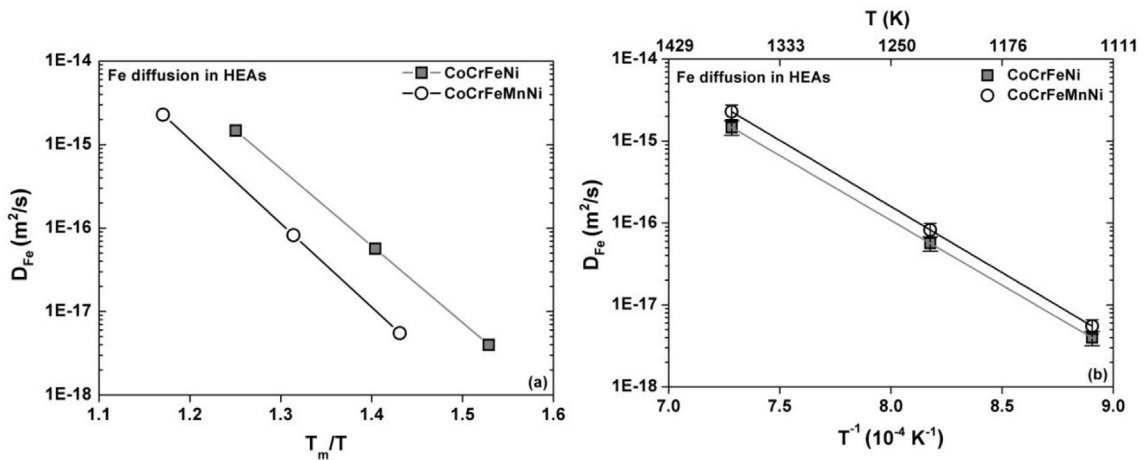


Fig. 11. Arrhenius diagrams for Fe diffusion in CoCrFeNi and CoCrFeMnNi alloys plotted using (a) the inverse homologous temperature or (b) the inverse absolute temperature.

times (161 h) and both profiles are presented in Fig. 12a. The penetration profiles obtained are similar for both the measurements and the determined diffusion coefficients are similar. The

first branch of the penetration profiles at all temperatures is linear in the coordinates of the logarithm of the tracer concentration against  $x^2$  confirming the presence of a corresponding bulk

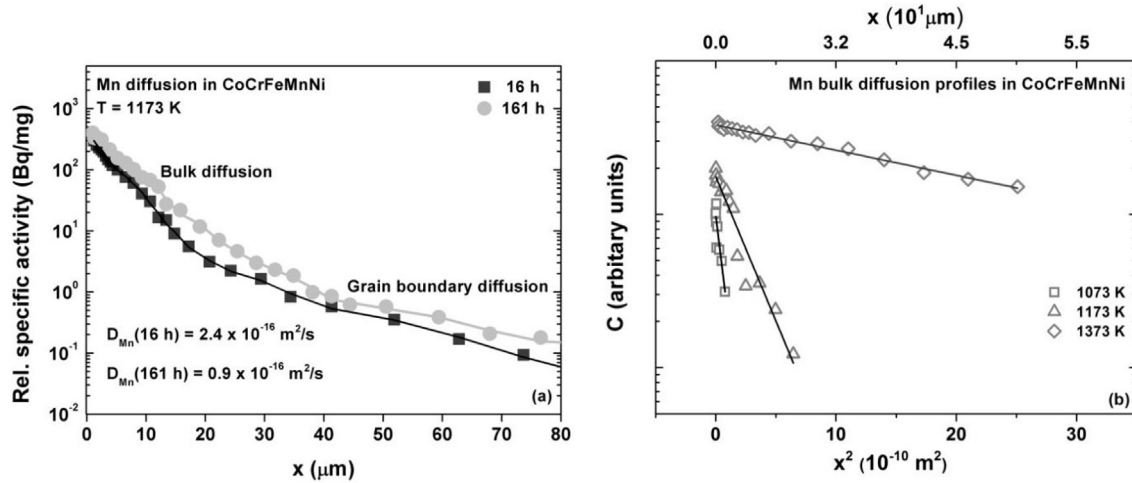


Fig. 12. (a) Concentration profiles of Mn tracer diffusion measured at 1173 K and (b) the first branch (bulk diffusion) of composition profile data plotted for various temperatures.

diffusion contribution (Fig. 12b).

#### 4. Discussion

High configurational entropy in multi-principal element alloys is believed to lend the phase stability to HEAs. However, phase separation at a nano-scale has been observed in HEAs [25,26], even though XRD evinces a single phase structure. Such a microstructure can cause complexity in assessing diffusion behaviour. Therefore, CoCrFeNi and CoCrFeMnNi HEA samples were analyzed using APT (Figs. 2 and 3), which confirms (from the binomial frequency distribution) that no phase separation is seen in both CoCrFeNi and CoCrFeMnNi at near-atomic scale in the present case. Further, it has been conclusively shown in Ref. [12] that the FCC structure of CoCrFeNi and CoCrFeMnNi HEAs are thermally stable during the temperature and time employed for the diffusion annealing.

##### 4.1. Bulk diffusion in CoCrFeNi and CoCrFeMnNi HEAs

The temperature dependence of the diffusion coefficients in HEAs is found to follow Arrhenius behaviour,

$$D = D_0 \exp\left(-\frac{Q}{RT}\right) \quad (3)$$

where  $D_0$  is the pre-exponential factor,  $Q$  is the activation energy, and  $R$  is the universal gas constant. The Arrhenius parameters (i.e.,  $D_0$  and  $Q$ ) for diffusion of all tracers in both CoCrFeNi and CoCrFeMnNi HEAs and other FCC matrices are given in Table 2. The determined Arrhenius dependencies for diffusion of all tracers in CoCrFeNi and CoCrFeMnNi are plotted in Fig. 13a and Fig. 13b, respectively. It has to be noted that although Ni bulk diffusion is not

measured in the present work, the Ni diffusion coefficients (and the derived parameters) in Ref. [12] are presented in this manuscript at various instances for comparison and overall assessment of bulk diffusion in the two alloys.

The diffusivities of all tracers in CoCrFeNi do not differ by more than an order of magnitude, although Ni diffusion is the slowest among all (Fig. 13a). The variation of diffusivities in CoCrFeNi can be expressed as  $D_{\text{Ni}} \leq D_{\text{Co}} < D_{\text{Fe}} \leq D_{\text{Cr}}$  at higher temperatures and  $D_{\text{Ni}} \leq D_{\text{Co}} \leq D_{\text{Fe}} \leq D_{\text{Cr}}$  at lower ones, which is in agreement with the trend reported for self diffusion of constituents in FCC Fe-Ni-Cr alloy system [27]. This has been correlated with the electronic structure of the elements as the diffusivities are found to decrease with increase in number of 3d electrons (Cr-4, Fe-6, Co-7, Ni-8) [27]. The exact contribution of the electronic structure during diffusion of atoms calls for the calculation of inter-atomic potentials at the saddle point configuration. Correlation with electronic structure is not evident in CoCrFeMnNi (Fig. 13b). Although, at lower temperatures diffusivities follow the order  $D_{\text{Ni}} < D_{\text{Co}} < D_{\text{Fe}} < D_{\text{Cr}}$ , diffusivity of Co reduces relative to Ni at higher temperatures. Mn shows the highest diffusion rates in CoCrFeMnNi even though it has higher number of 3d electrons than Cr. This can be attributed to the significantly lower melting point of Mn among other constituents, which results in lower energy required to create an atom-vacancy pair. Within the investigated temperature interval, the maximum difference between the diffusion coefficients of various constituents in both HEAs does not exceed an order of magnitude. In the previous work on interdiffusion in CoCrFeMnNi [8], almost parallel Arrhenius lines for the different constituents have been reported; however, the direct measurements do not support those estimates. This fact substantiates contributions of both, the energy barriers and the frequency factors to diffusion in HEAs.

The activation energies of different elements in these two HEAs can be rationalized by considering relative thermodynamic interaction of an element  $i$  with other constituents. Table 3 lists the mixing enthalpies of all binary pairs constituting the equiatomic HEAs under investigation [28]. We calculate the average enthalpy of mixing of each constituent with all other individual components ( $\Delta H_{\text{avg}}^i$ ) in both 4 and 5 component alloys, from the following expression:

$$\Delta H_{\text{avg}}^i = \frac{\sum_{j \neq i}^n \Delta H_{\text{mix}(ij)}}{n} \quad (4)$$

Table 2

Activation energy ( $Q$ ) and the pre-exponential factors ( $D_0$ ) for bulk diffusion of the constituents in CoCrFeNi and CoCrFeMnNi.

Tracer	Diffusion in CoCrFeNi		Diffusion in CoCrFeMnNi	
	$Q$ (kJ/mol)	$D_0$ (m <sup>2</sup> /s)	$Q$ (kJ/mol)	$D_0$ (m <sup>2</sup> /s)
Co	240 ± 20	$4.6_{-3.9}^{+26} \times 10^{-7}$	270 ± 22	$1.6_{-1.6}^{+69} \times 10^{-5}$
Cr	323 ± 5	$4.2_{-0.8}^{+0.9} \times 10^{-3}$	313 ± 13	$2.4_{-2.1}^{+1.9} \times 10^{-3}$
Fe	303 ± 3	$4.9_{-1.3}^{+1.8} \times 10^{-4}$	309 ± 11	$1.3_{-1.1}^{+9} \times 10^{-3}$
Mn	—	—	272 ± 13	$1.6_{-1.1}^{+26} \times 10^{-4}$
Ni	253 ± 8	$1.1_{-0.4}^{+0.6} \times 10^{-6}$	304 ± 9	$6.2_{-1.5}^{+18} \times 10^{-4}$

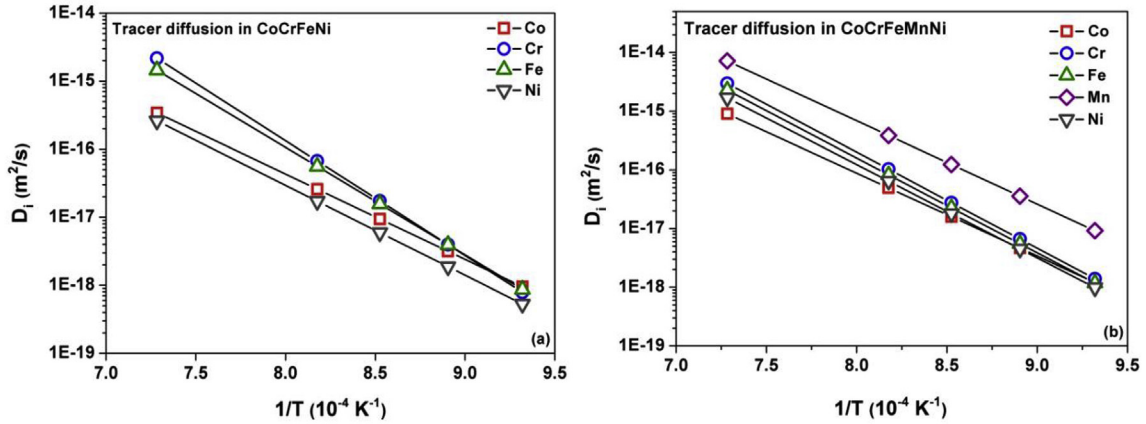


Fig. 13. Temperature dependence of bulk diffusion of all constituents in a) CoCrFeNi b) CoCrFeMnNi. Ni diffusion is slowest in CoCrFeNi, while the Mn diffusion rate is highest in CoCrFeMnNi.

Table 3  
Enthalpy of mixing for binary pairs of the multicomponent alloys [28].

Binary System	$\Delta H_{mix}$ (kJ/mol)	Binary system	$\Delta H_{mix}$ (kJ/mol)
Co-Cr	-4	Cr-Mn	2
Co-Fe	-1	Cr-Ni	-7
Co-Mn	-5	Fe-Mn	0
Co-Ni	0	Fe-Ni	-2
Cr-Fe	-1	Mn-Ni	-8

Here,  $\Delta H_{mix(ij)}$  is the binary enthalpy of mixing of *i*th and *j*th elements. For e.g.,  $\Delta H_{avg}^{Co}$  is 1.7 and 2.5 kJ/mol for CoCrFeNi and CoCrFeMnNi, respectively. Fig. 14a and b presents the values of  $\Delta H_{avg}^i$  and  $Q_i$  for different elements in CoCrFeNi and CoCrFeMnNi, respectively. The activation energies for Co, Cr and Ni diffusion in CoCrFeNi vary in the order  $Q_{Co} < Q_{Ni} < Q_{Cr}$  which correlates well with the trends in their respective average enthalpy of mixing as  $\Delta H_{avg}^{Cr} < \Delta H_{avg}^{Ni} < \Delta H_{avg}^{Co}$  (Fig. 14a). A more negative value of  $\Delta H_{avg}^i$  suggests a relatively stronger binding of the element with other constituents and hence an increased activation barrier for diffusion. The only exception to this trend in CoCrFeNi is Fe, which has a less negative  $\Delta H_{avg}^i$  value but exhibits higher  $Q$ . Such a correlation with the activation energy parameters is slightly less evident in CoCrFeMnNi (Fig. 14b). Both Co and Mn have similar values of  $\Delta H_{avg}^i$  (-2.5 and -2.75 kJ/mol, respectively) and show

comparable activation energies of diffusion (270 and 272 kJ/mol, respectively). The  $\Delta H_{avg}^i$  for Fe, Cr and Ni follows the order  $\Delta H_{avg}^{Fe} < \Delta H_{avg}^{Cr} < \Delta H_{avg}^{Ni}$ , however they exhibit similar values of  $Q$ . It is proposed here that the BCC structure and higher melting point of Cr may additionally contribute to higher  $Q$  values for Cr despite lower  $\Delta H_{avg}^{Cr}$ . However, we believe that the systematic diffusion experiments in non-equiatomeric quaternary and quinary HEAs with varying concentrations of Cr and Fe can throw more light on this intriguing behaviour.

Equation (3) substantiates that the pre-exponential factor,  $D_0$ , has a strong impact on the diffusion rates, too. Co and Ni exhibit low values of  $D_0$  while Fe and Cr have shown high  $D_0$  in both HEAs (Table 2).  $D_0$  is usually expressed as  $D_0 = gfa^2v_0 \exp(\Delta S/R)$  [24], where  $g$  is a geometric factor,  $f$  is the correlation factor,  $a$  is the lattice parameter,  $v_0$  is the attempt frequency, and  $\Delta S$  is the diffusion entropy. For a vacancy mediated diffusion mechanism, the correlation factor arises due to an increased probability of reversed atomic jumps that result in reduced diffusion distances with respect to those for a completely random atom movement. The value of  $f$  is a constant for bulk diffusion in a given crystal structure ( $f \sim 0.787$  for FCC). Thus, for a given alloy, except for  $\Delta S$ , other parameters remain constant for diffusion of all constituent elements.  $\Delta S$  is the change of the entropy of lattice vibrations originating from a constrained movement of the diffusing atom through a saddle point configuration [29,30].  $\Delta S$  has two contributions namely,

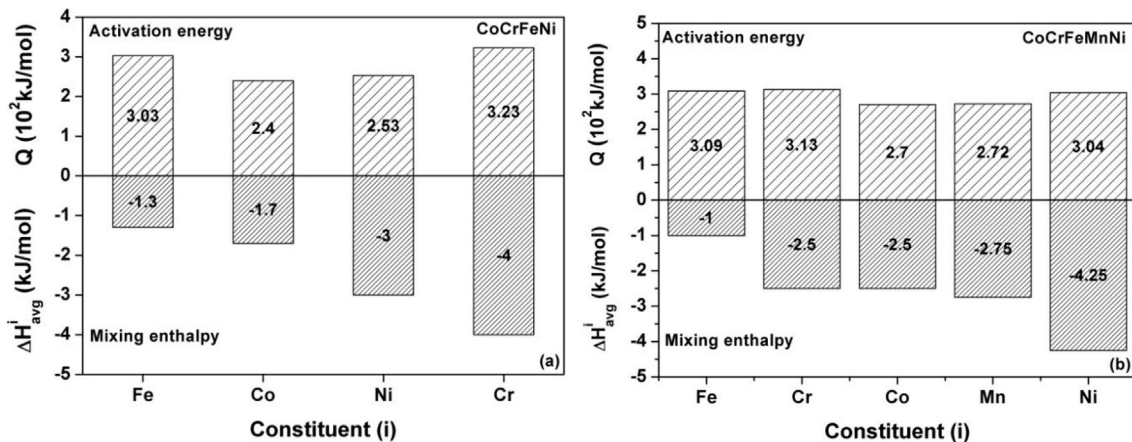


Fig. 14. Correlation between the average enthalpy of mixing ( $\Delta H_{avg}^i$ ) and the activation energy for bulk diffusion ( $Q$ ) for all constituents in a) CoCrFeNi and b) CoCrFeMnNi.

vibrational and configurational. A change of the vibrational component of  $\Delta S$  will depend upon the lattice stiffness and the bond lengths of the diffusing atom in the matrix, while the coordination number of the diffusing atom in the lattice determines the configurational part [29]. Thus, the low values of  $\Delta S$  for Co and Ni in CoCrFeNi and CoCrFeMnNi call for detailed investigations of the elastic constants and short range order, e.g., using first principle calculations.

An interesting feature observed during comparison of bulk tracer diffusivities in CoCrFeNi and CoCrFeMnNi HEAs is the appearance of a cross-over temperature ( $T_c$ ) for Co (Fig. 6), which is similar to what has been reported earlier for Ni diffusion [12]. The values of  $T_c$  are 970 and 1020 K for Ni and Co, respectively, above which their diffusion rates in CoCrFeMnNi alloys are higher than in CoCrFeNi alloys. However, as shown in Figs. 10 and 11, the cross-over temperature is not observed for Fe and Cr diffusion in these HEAs. This behaviour can be rationalized if the effect of Mn addition on CoCrFeNi is considered. The melting point of CoCrFeNi is 1717 K, which reduces to 1607 K in CoCrFeMnNi. This implies that at any given absolute temperature, the equilibrium vacancy concentration is higher in CoCrFeMnNi, which will tend to increase the rate of substitutional diffusion. However, addition of Mn will also cause a change in the  $\Delta H_{avg}^i$  values for each constituent. This change in average enthalpy is defined as  $\Delta H_{avg}^{i,diff} = \Delta H_{avg}^{i,CoCrFeMnNi} - \Delta H_{avg}^{i,CoCrFeNi}$  and these values are presented in Fig. 15a. In the case of Co,  $\Delta H_{avg}^{Co}$  is 1.7 and 2.5 kJ/mol for CoCrFeNi and CoCrFeMnNi, respectively. So  $\Delta H_{avg}^{Co,diff} = -2.5 - (-1.7) = -0.8$  kJ/mol. Thus,  $\Delta H_{avg}^{Co}$  becomes more negative with the addition of Mn, which implies that Co binding is stronger in CoCrFeMnNi in comparison to CoCrFeNi. A similar behaviour is seen for Ni as well, where  $\Delta H_{avg}^{Ni}$  changes from 0.0 kJ/mol for CoCrFeNi to  $-4.25$  kJ/mol for CoCrFeMnNi [12]. It results from the fact that the Ni-Mn and Co-Mn pairs have the strongest interaction among the different binaries

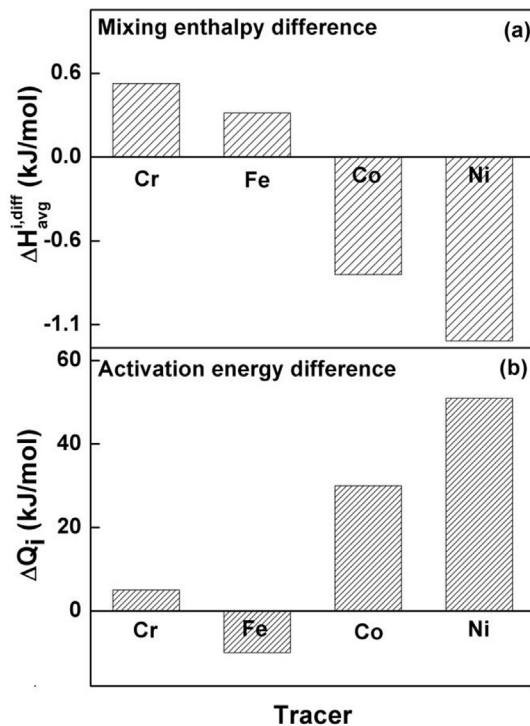


Fig. 15. a) Change in average enthalpy of mixing for each constituent ( $\Delta H_{avg}^{i,diff}$ ) between the HEA matrices of CoCrFeNi and CoCrFeMnNi. b) Change in activation energy ( $\Delta Q_i$ ) for diffusion of corresponding constituent between CoCrFeNi and CoCrFeMnNi.

(Table 3). Thus, the addition of Mn causes two opposite effects on Co and Ni diffusion rates, namely, an increase of the  $\Delta H_{avg}^i$  value and a reduction of the alloy melting point. This combination leads finally to the appearance of a cross-over temperature. As shown in Fig. 15a,  $\Delta H_{avg}^i$  becomes less negative for Cr and Fe upon Mn addition to CoCrFeNi, which implies that they are less strongly bound in CoCrFeMnNi. Thus, the non-existence of the two opposite effects of Mn addition on Cr and Fe diffusion explains why the cross-over temperature is not observed in case of Cr and Fe.

Fig. 15b reveals the change of the activation energy ( $\Delta Q_i = Q_i^{CoCrFeMnNi} - Q_i^{CoCrFeNi}$ ) for Co, Cr, Fe and Ni as a result of the addition of Mn to CoCrFeNi in equiatomic proportion. The comparison of Fig. 15a and b indicates an interesting trend. It is seen that  $\Delta Q_i$  is significant for Co and Ni and these elements show the largest negative  $\Delta H_{avg}^i$ , too. Thus, the increased activation energy of Co and Ni diffusion in CoCrFeMnNi correlates with their more negative  $\Delta H_{avg}^i$  value after Mn addition. The corresponding changes of  $\Delta Q_i$  for Fe and Cr are minimal, which corroborates with the fact that  $\Delta H_{avg}^{Cr}$  and  $\Delta H_{avg}^{Fe}$  are not altered significantly from CoCrFeNi and CoCrFeMnNi.

Figs. 6, 10 and 11 highlight the fact that if the inverse of the homologous temperature,  $T_m/T$ , is used for comparison of the diffusion rates of Co, Cr and Fe in CoCrFeNi and CoCrFeMnNi, there is an obvious trend of diffusion retardation with an increased number of the components, i.e. with the increased configurational entropy. However, this tendency does not exist if the absolute temperature scale is used for comparison. This behaviour matches the results on Ni diffusion in HEAs reported in our earlier study [12].

#### 4.2. Bulk diffusion in HEAs and other FCC matrices

The bulk tracer diffusion behaviour of the constituent elements in CoCrFeNi and CoCrFeMnNi, discussed in an earlier section, reflects the fact that the influence of the configurational entropy on diffusion in HEAs is not straightforward. To elaborate further the effect of mixing entropy, the diffusivities of Co, Cr, Fe and Mn in different FCC matrices are compared on the homologous temperature scale (Fig. 16). In order to simplify the interpretation, the diffusion coefficients  $D$ 's are not rescaled as  $D^* = D \left( \frac{M}{kT_m a^2} \right)^{1/2}$ , see e.g. Ref. [10], since the relative positions of different data lines would be hardly affected but the main message is more straightforward when the measured diffusivities are plotted (here  $M$  is the composition-weighted mean of the atomic masses in the alloy and  $a$  is the corresponding lattice constant [10]).

Co diffusion in CoCrFeNi and CoCrFeMnNi is slower when compared to that in pure Co (Fig. 16a) [31,32]. Decelerated rates of the atomic transport are observed for Cr [27,33] and Fe [27,34] as the number of components increase from pure Fe to the quinary alloy (Fig. 16b and c, respectively). Mn bulk-diffusion is slower in the quaternary and quinary HEAs relative to pure Mn (Fig. 16d) [32,35]. It can thus be inferred that with an increasing number of components in the alloys, when compared against the inverse homologous temperature, the diffusion rates in the FCC matrix are retarded.

Diffusion of all constituents in the quinary alloy is characterized by higher normalized activation enthalpies  $Q^*$  ( $=Q/RT_m$ ) when compared with lower component alloys. This is exemplified for Co and Cr diffusion in Fig. 17a and b, respectively. The increase of  $Q^*$  can be attributed to a depression of the melting point caused by the Mn addition and it gets further enhanced for Co diffusion due to the increase of  $\Delta H_{avg}^i$ . In case of CoCrFeNi, lower  $\Delta S$  values are observed for Co diffusion in CoCrFeNi (Fig. 17a), which accounts for its lower

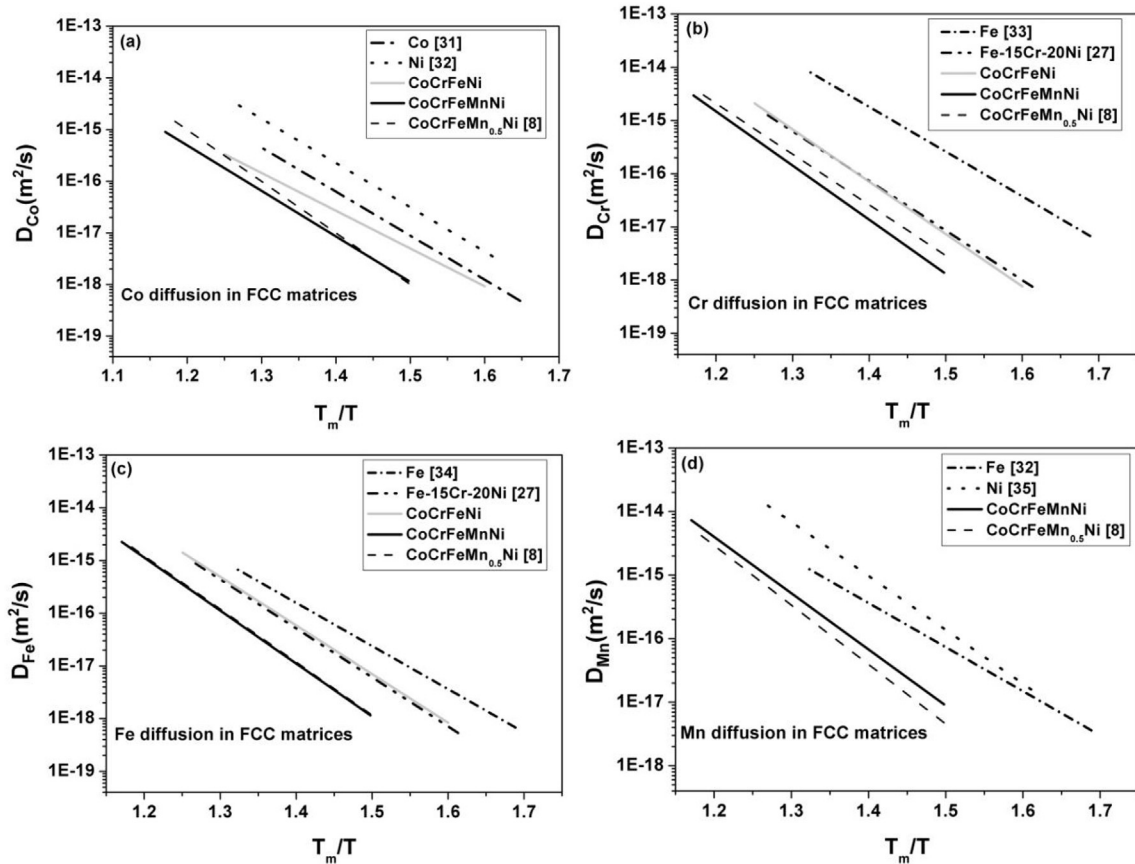


**Fig. 16.** Decelerated diffusion rates in HEAs on a homologous temperature scale a) Co diffusion in Co, Ni and CoCrFeMn<sub>0.5</sub>Ni, b) Cr diffusion in Fe, Fe-15Cr-20Ni and CoCrFeMn<sub>0.5</sub>Ni, c) Fe diffusion in Fe, Fe-15Cr-20Ni and CoCrFeMn<sub>0.5</sub>Ni and d) Mn diffusion in Fe, Ni and CoCrFeMn<sub>0.5</sub>Ni.

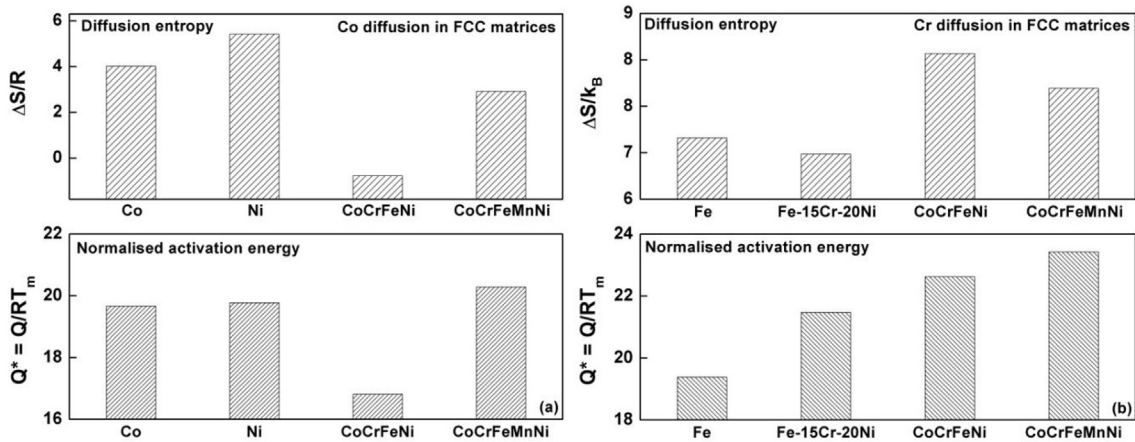


**Fig. 17.** Normalized activation energy ( $Q^* = Q/RT_m$ ) and diffusion entropy ( $\Delta S/k_B$ ) (derived from pre-exponential factor,  $D_0$ ) for diffusion of Co and Cr in HEAs and other FCC matrices. The references for  $Q$  and  $D_0$  for other FCC matrices are the same as mentioned in Fig. 17 to compare their diffusion rates with HEAs.

diffusivities when compared to other FCC matrices. Retardation of Cr diffusion rates in CoCrFeNi can be attributed to a higher  $Q^*$  value (Fig. 17b). The attributes of Co diffusion in CoCrFeNi and CoCrFeMnNi HEAs exhibit similarities with the Ni diffusion behaviour reported in Ref. [12].

When compared on the absolute temperature scale, the increased configurational entropy does not follow the reduction in diffusivities as exemplified for Co and Cr diffusion in different

matrices (Fig. 18a and b). A similar behaviour is seen for Fe and Mn diffusion as well (not shown here).

The reversal in diffusivity trends between the homologous and absolute temperature scales and the existence of a cross-over temperature for Co and Ni diffusion in HEAs allows deducing that the original hypothesis of sluggish diffusion in HEAs is not valid for the alloys studied in this work. Experimental investigations of tracer diffusion in others HEA systems are essential to obtain

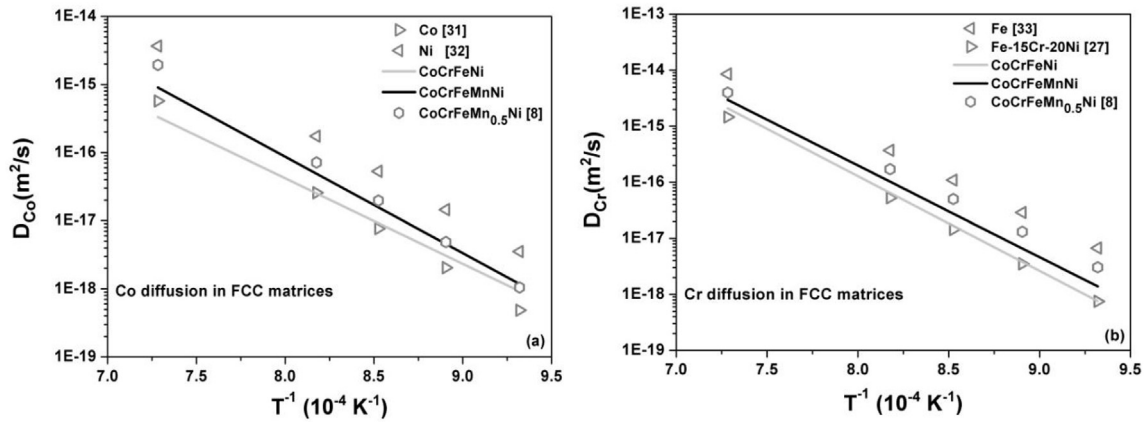


Fig. 18. Decelerated diffusion rates in HEAs on the absolute temperature scale a) Co diffusion in Co, Ni and CoCrFeMn<sub>0.5</sub>Ni, b) Cr diffusion in Fe, Fe-15Cr-20Ni and CoCrFeMn<sub>0.5</sub>Ni.

deeper insights into the effect of increasing the number of elements. However, a major challenge would be to identify HEAs having a single phase composition with a sufficiently high thermal stability.

#### 4.3. “Compensation law” for diffusion in HEAs

In the limited literature available for diffusion in HEAs (Table 1), the relationship between  $D_0$  and  $Q$  has not been examined so far. In Fig. 19, the pre-exponentials factors  $D_0$  for diffusion of all constituents in CoCrFeNi and CoCrFeMnNi are plotted against the corresponding values of the activation enthalpy  $Q$ . An almost perfectly linear relationship is seen, the solid line, which is determined using a least square fit as

$$\ln D_0 = (-42.5 \pm 1) + (0.116) \cdot Q \quad (5)$$

Here  $D_0$  and  $Q$  are expressed in  $\text{m}^2/\text{s}$  and  $\text{kJ}/\text{mol}$ , respectively. Such an empirical linear correlation between  $D_0$  and  $Q$  is often called as compensation law or Meyer–Neldel rule and it is observed for wide variety of thermally activated processes such as grain boundary and interfacial diffusion, grain boundary migration, dislocation movement and electron transport [36]. The origin of the Meyer–Neldel rule lies in the multi-excitation process to overcome the activation barrier [37]. To illustrate, diffusion of an atom proceeds via a saddle point configuration or an activated state, for which thermal fluctuations (or excitations) are required. When the

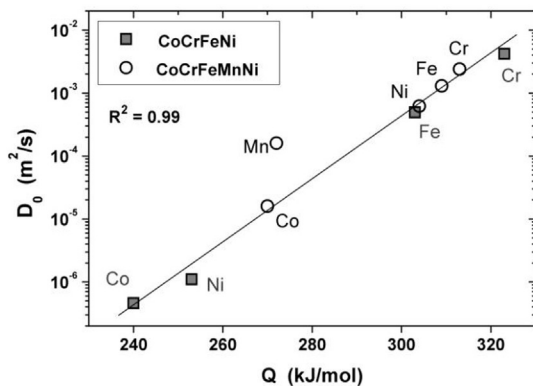
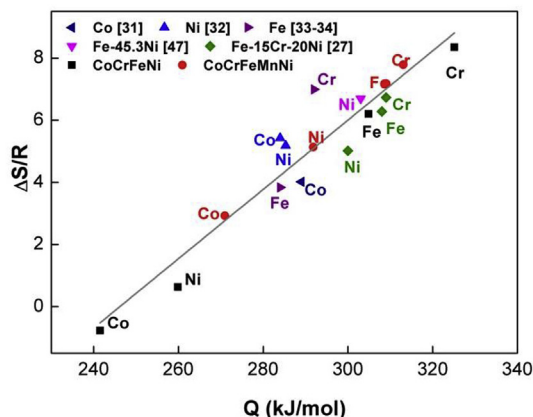


Fig. 19. The pre-exponential factors ( $D_0$ ) for bulk diffusion of the constituent elements in CoCrFeNi (squares) and CoCrFeMnNi (circles) as a function of the corresponding activation energy  $Q$ . All elements except of Mn reveal an almost linear dependence, obtained using least square fit, of  $\ln D_0$  vs.  $Q$  (solid line).

activation energy to reach the transition is sufficiently high, multiple excitations become necessary to surmount the energy barrier [38]. The number of ways in which these fluctuations can manifest gives rise to an entropic contribution and thus increases diffusion entropy ( $\Delta S$ ) and consequently  $D_0$ . In other words, the high energy barrier in a thermally activated process gets “compensated” by increasing the number of paths to the activated state. The coefficient of  $Q$  in Eq. (5) is equal to  $1000/RT^*$ , where  $T^*$  is the compensation temperature ( $T^*$ ). The values of  $T^*/T_m$  for CoCrFeNi and CoCrFeMnNi turned out to be 0.60 and 0.65, respectively, which fall in the range generally observed for polycrystalline alloys [39].

Further, two important points regarding the compensation law need to be noted. Firstly, although attempts have been made to support physical explanations of Meyer–Neldel rule attempted through atomistic simulations [40], Eq. (5) is still an empirical relation and need not be universally applicable [41]. As seen in Fig. 19, the linear relationship is valid for all elements except Mn in CoCrFeMnNi. Mn reveals larger  $D_0$  as it would be followed from Eq. (5), by almost an order of magnitude. This fact indicates probably a specific situation for diffusion of Mn atoms in CoCrFeMnNi. Note that Mn is the fastest diffusing element in the alloy and its concentration is above the percolation threshold for diffusion in a binary mixture [42] (if all other elements will be considered as belonging effectively to the same type in a mean-field approach). Secondly, compensation only implies that the increased activation barrier for diffusion can be moderated by creating additional thermal excitations (higher  $\Delta S$ ), which increase  $D_0$ . It does not, however, necessitate that the governing factors are the same for  $D_0$  and  $Q$  for diffusion or any thermally activated process. The deviations for Mn from the ‘general trend’ do support this point of view.

The relation between the values of  $Q$  and  $\Delta S$  is further explored in Fig. 20 by plotting the values of activation entropies,  $\Delta S/R$ , for Co, Cr, Fe and Mn diffusion in HEAs and other FCC matrices as function of the corresponding activation energies  $Q$ . The value of  $\Delta S/R$  is calculated from the expression for  $D_0$  given earlier by taking an average lattice parameter of 0.355 nm, constant geometric and correlation factors (1 and 0.787, respectively) for the FCC lattice and taking  $\nu_0$  as the Debye frequency ( $10^{13} \text{ s}^{-1}$ ). Fig. 20 substantiates the existence of a linear dependence of  $\Delta S/R$  vs.  $Q$  for a broad spectrum of FCC alloys which could be derived from Eq. (5). It is important to note that Fig. 20 shows the results of many independent measurements, which thus excludes any systematic error. The linearity of  $D_0$  vs.  $Q$  dependence for HEAs and lower component FCC systems presents an intriguing aspect. It hints that an increased number of



**Fig. 20.** Diffusion entropy  $\Delta S/R$  (derived from the pre-exponential factor,  $D_0$ , see text) as a function of the corresponding activation energy for diffusion of the constituent elements in binary, ternary and high-entropy alloys. Linear relationship obtained using least square fit is evident [47].

components in HEAs do not alter the atomistic processes of diffusion as long as the crystal structure remains same. This also presents the need to delve deeper into the crystal structure of HEAs and decipher the uniqueness that a multi-element matrix really brings in.

#### 4.4. “Sluggish” diffusion in HEAs – number of elements or atomic configuration?

The bulk diffusion results presented above show that diffusion needs not be sluggish in HEAs. Even the results of the very first study on diffusion in HEAs [8], when analyzed on the absolute temperature scale, revealed that the measured diffusivities are not very different from those in pure elements or binary alloys [7]. Miracle and Senkov [7] also argued that most of the experimental investigations that supported the claim of sluggish diffusion in HEAs were based on secondary observations. In fact, some of the recent studies have hinted towards the non-sluggishness of diffusion in HEAs too [43,44]. So, does it mean that the premise of sluggish diffusion in HEAs is flawed? To address this question, a distinction needs to be made between the number of elements and the configurations of elements in an alloy. To give a simple illustration we compare the  $\text{CoCrFeMn}_{0.5}\text{Ni}$  and  $\text{CoCrFeMn}_1\text{Ni}$  HEAs (the sub-index “1” can be omitted in the latter case, we keep it just for clarity). In fact, the number of elements remains the same, whereas their configuration (or composition) changes. However, upon alloying  $\text{CoCrFeNi}$  with Mn (to the compositions  $\text{CoCrFeMn}_{0.5}\text{Ni}$  and  $\text{CoCrFeMnNi}$ ), we change the number of elements as well as their configuration. The implication of this classification is that when a new element is added to a multicomponent system, thermodynamic changes introduced are much larger and will certainly depend on the type of the element added. For example,  $\text{CoCrFeNiAl}$  and  $\text{CoCrFeNiMn}$  have similar configurational entropies, but are significantly different in their structures (predominantly BCC and exclusively FCC, respectively) and properties [45]. When only the configuration of the constituents is changed, the thermodynamic properties of the system vary by a smaller extent and the influence of configurational entropy can be brought out in a more lucid way. The “sluggish” diffusion effect was apparently proposed to imply the effect of merely increasing the number of elements and could not explicitly take into account the influence of the type of the component added. Therefore, we believe that a more appropriate way of presenting the core concept of “sluggish”

diffusion in HEAs would be to define it in terms of the changes of the configurational entropy while retaining the same alloy constituents. For example, Yang et al. [46] studied the crystallization kinetics in  $\text{Zr}_{1.2}\text{Ti}_1\text{Cu}_1\text{Ni}_1\text{Be}_1$  and  $\text{Zr}_{41.2}\text{Ti}_{13.8}\text{Cu}_{12.5}\text{Ni}_{10}\text{Be}_{22.5}$  bulk metallic glasses, where former showed a higher stability. Thus, a way forward for deeper understanding of diffusion in HEAs would be to determine the bulk diffusivities of non-equiatomic and equiatomic HEAs with the same constituents.

## 5. Conclusions

The radiotracer method has been applied to determine the tracer diffusion coefficients of Co, Cr, Fe and Mn in the  $\text{CoCrFeNi}$  and  $\text{CoCrFeMnNi}$  HEAs. Two contributions to the atomic transport kinetics are observed in the penetration profiles for both quaternary and quinary polycrystalline alloys, and the bulk diffusion coefficients are accurately determined.

Ni shows the lowest diffusion rates in both  $\text{CoCrFeNi}$  and  $\text{CoCrFeMnNi}$ , while Mn diffuses fastest in  $\text{CoCrFeMnNi}$ . The activation energy ( $Q$ ) of Co diffusion is significantly higher in  $\text{CoCrFeMnNi}$  than in  $\text{CoCrFeNi}$  and can be correlated with the more negative average mixing enthalpy ( $\Delta H_{\text{avg}}^i$ ) in the quinary alloy. The  $Q$  value for Fe and Cr are similar in both HEAs in accordance with their similar values of  $\Delta H_{\text{avg}}^i$  in both alloys. A cross-over temperature, above which diffusion is faster in the  $\text{CoCrFeMnNi}$  alloy relative to  $\text{CoCrFeNi}$ , is observed for Co diffusion. It is attributed to two opposite effects of the Mn addition, namely, a depression of the melting point and a more negative value of  $\Delta H_{\text{avg}}^i$  of the constituents in the quinary alloy.

Decelerated bulk diffusion rates have been measured in HEAs relative to the FCC matrices with a smaller number of principal elements when the homologous temperature is used for comparison. Both the energy barriers and the entropy factors (derived from  $D_0$ ) contribute to the lower diffusion rates. A tendency of decreasing diffusivities with increasing number of components is not evident when the absolute temperature scale is used for comparison of the diffusion rates. Our results conclusively substantiate that diffusion should not be assumed sluggish in HEAs due to the mere increase of the number of elements; in fact the type of elements plays a more pronounced role. We suggest that a more appropriate way to reformulate the “sluggish-diffusion” core effect in HEAs to the extent that it is classified in terms of the changes in the configurational entropy while retaining the same alloy constituents.

## Acknowledgements

Financial support from the Growing Spine Foundation, DFG, project DI 1419/13-1, is acknowledged. M. Vaidya would also like to thank DAAD for providing a scholarship to carry out tracer diffusion experiments at University of Münster, Germany. GW acknowledges partial support by DFG. The authors also acknowledge the support of DAAD in facilitating the RWTH-IITM strategic partnership program.

## References

- [1] M.C. Gao, P.K. Liaw, J.W. Yeh, Y. Zhang, *High-Entropy Alloys*, Springer International Publishing, 2016.
- [2] B.S. Murty, J.W. Yeh, S. Ranganathan, *High-entropy Alloys*, Butterworth-Heinemann, 2014.
- [3] Z. Li, K.G. Pradeep, Y. Deng, D. Raabe, C.C. Tasan, Metastable high-entropy dual-phase alloys overcome the strength–ductility trade-off, *Nature* 534 (2016) 227–230.
- [4] D. Li, Y. Zhang, The ultrahigh charpy impact toughness of forged  $\text{AlxCoCrFeNi}$  high entropy alloys at room and cryogenic temperatures, *Intermetallics* 70 (2016) 24–28.
- [5] T.M. Butler, M.L. Weaver, Oxidation behavior of arc melted  $\text{AlCoCrFeNi}$  multi-

- component high-entropy alloys, *J. Alloy. Compd.* 674 (2016) 229–244.
- [6] J.J. Zhang, X.L. Yin, Y. Dong, Y.P. Lu, L. Jiang, T.M. Wang, T.J. Li, Corrosion properties of  $\text{Al}_x\text{CoCrFeNiTi}_{0.5}$  high entropy alloys in 0.5M  $\text{H}_2\text{SO}_4$  aqueous solution, *Mater. Res. Innovat.* 18 (2014) 756–760.
- [7] D.B. Miracle, O.N. Senkov, A critical review of high entropy alloys and related concepts, *Acta Mater.* 122 (2017) 448–511.
- [8] K.Y. Tsai, M.H. Tsai, J.W. Yeh, Sluggish diffusion in Co-Cr-Fe-Mn-Ni high-entropy alloys, *Acta Mater.* 61 (2013) 4887–4897.
- [9] K. Kulkarni, G.P.S. Chauhan, Investigations of quaternary interdiffusion in a constituent system of high entropy alloys, *AIP Adv.* 5 (2015) 97162.
- [10] D.L. Beke, G. Erdélyi, On the diffusion in high-entropy alloys, *Mater. Lett.* 164 (2016) 111–113.
- [11] M. Zajusz, J. Dąbrowa, M. Danielewski, Determination of the intrinsic diffusivities from the diffusion couple experiment in multicomponent systems, *Scr. Mater.* 138 (2017) 48–51.
- [12] M. Vaidya, S. Trubel, B.S. Murty, G. Wilde, S.V. Divinski, Ni tracer diffusion in CoCrFeNi and CoCrFeMnNi high entropy alloys, *J. Alloy. Compd.* 688 (2016) 994–1001.
- [13] A.R. Allnatt, T.R. Paul, I.V. Belova, G.E. Murch, A high accuracy diffusion kinetics formalism for random multicomponent alloys: application to high entropy alloys, *Philos. Mag.* 96 (2016) 2969–2985.
- [14] T.R. Paul, I.V. Belova, G.E. Murch, Analysis of diffusion in high entropy alloys, *Mater. Chem. Phys.* (2017) 4–11.
- [15] M. Vaidya, K.G. Pradeep, B.S. Murty, G. Wilde, S.V. Divinski, Radioactive isotopes reveal a non sluggish kinetics of grain boundary diffusion in high entropy alloys, *Sci. Rep.* (2017) 1–11.
- [16] J. Dąbrowa, W. Kucza, G. Cieslak, T. Kulik, M. Danielewski, J.W. Yeh, Interdiffusion in the FCC-structured Al-Co-Cr-Fe-Ni high entropy alloys: experimental studies and numerical simulations, *J. Alloy. Compd.* 674 (2016) 455–462.
- [17] I. Basu, K.G. Pradeep, C. Miessen, L.A. Barrales-Mora, T. Al-Samman, The role of atomic scale segregation in designing highly ductile magnesium alloys, *Acta Mater.* 116 (2016) 77–94.
- [18] S. Mandal, K.G. Pradeep, S. Zaefferer, D. Raabe, A novel approach to measure grain boundary segregation in bulk polycrystalline materials in dependence of the boundaries' five rotational degrees of freedom, *Scr. Mater.* 81 (2014) 16–19.
- [19] M.P. Moody, L.T. Stephenson, A.V. Ceguerra, S.P. Ringer, Quantitative binomial distribution analyses of nanoscale like-solute atom clustering and segregation in atom probe tomography data, *Microsc. Res. Tech.* 71 (2008) 542–550.
- [20] N. Mattern, J.H. Han, K.G. Pradeep, K.C. Kim, E.M. Park, D.H. Kim, Y. Yokoyama, D. Raabe, J. Eckert, Structure of rapidly quenched  $(\text{Cu}_{0.5}\text{Zr}_{0.5})_{100-x}\text{Ag}_x$  alloys ( $x = 0-40$  at.%), *J. Alloy. Compd.* 607 (2014) 285–290.
- [21] A. Paul, T. Laurila, V. Vuorinen, S.V. Divinski, *Thermodynamics, Diffusion and the Kirkendall Effect in Solids*, Springer International Publishing, 2014.
- [22] L.G. Harrison, Influence of dislocations on diffusion kinetics in solids with particular reference to the alkali halides, *Trans. Faraday Soc.* 57 (1961) 1191.
- [23] A.D. Le Claire, A. Rabinovitch, A.D.L.E. Claire, The analysis of grain boundary diffusion measurements, *Br. J. Appl. Phys.* 14 (1963) 351–414.
- [24] P. Shewmon, *Diffusion in Solids*, Springer International Publishing, 2016.
- [25] A. Manzoni, H. Daoud, R. Völkl, U. Glatzel, N. Wanderka, Phase separation in equiatomic AlCoCrFeNi high-entropy alloy, *Ultramicroscopy* 132 (2013) 212–215.
- [26] C.Y. Yu, X.D. Xu, M.W. Chen, C.T. Liu, Atomistic mechanism of nano-scale phase separation in fcc-based high entropy alloys, *J. Alloy. Compd.* 663 (2016) 340–344.
- [27] S. Rothman, L. Nowicki, G. Murch, Self-diffusion in austenitic Fe-Cr-Ni alloys, *J. Phys. F Met.* 10 (1980) 383.
- [28] A. Takeuchi, A. Inoue, Classification of bulk metallic glasses by atomic size difference, heat of mixing and period of constituent elements and its application to characterization of the main alloying element, *Mater. Trans.* 46 (2005) 2817–2829.
- [29] C. Wert, C. Zener, Interstitial atomic diffusion coefficients, *Phys. Rev.* 76 (1949) 1169–1175.
- [30] G.H. Vineyard, Frequency factors and isotope effects in solid state rate processes, *J. Phys. Chem. Solid.* 3 (1957) 121–127.
- [31] W. Bussmann, C. Herzig, W. Rempp, K. Maier, H. Mehrer, Isotope effect and self-diffusion in face-centred cubic cobalt, *Phys. Status Solidi.* 56 (1979) 87–97.
- [32] G. Neumann, C. Tuijn, *Self-diffusion and Impurity Diffusion in Pure Metals: Handbook of Experimental Data*, Elsevier, 2011.
- [33] A.W. Bowen, G.M. Leak, Solute diffusion in alpha- and gamma-iron, *Metall. Trans.* 1 (1970) 1695–1700.
- [34] T. Heumann, R. Imm, Self-diffusion and isotope effect in  $\gamma$ -iron, *J. Phys. Chem. Solid.* 29 (1968) 1613–1621.
- [35] R. Swalin, A. Martin, Solute diffusion in nickel-base substitutional solid solutions, *J. Met.* 8 (1956).
- [36] G. Gottstein, L.S. Shvindlerman, The compensation effect in thermally activated interface processes, *Interface Sci.* 6 (1998) 265–276.
- [37] A. Yelon, B. Movaghar, Microscopic explanation of the compensation (Meyer-Neldel) rule, *Phys. Rev. Lett.* 65 (1990) 618–620.
- [38] A. Yelon, B. Movaghar, H.M. Branz, Origin and consequences of the compensation (Meyer-Neldel) law, *Phys. Rev. B* 46 (1992) 12244–12250.
- [39] M.N. Magomedov, Compensation effects for the diffusion process, *High Temp.* 40 (2001) 142–144.
- [40] K. Shimakawa, M. Aniya, Dynamics of atomic diffusion in condensed matter: origin of the Meyer-Neldel compensation law, *Monatsh. Chem.* 144 (2013) 67–71.
- [41] R. Kirchheim, X.Y. Huang, A relationship between prefactor and activation energy for diffusion, *Phys. Status Solidi.* 144 (1987) 253–257.
- [42] H. Ouyang, B. Fultz, Percolation in alloys with thermally activated diffusion, *J. Appl. Phys.* 66 (1989) 4752–4755.
- [43] S.R. Reddy, S. Bapari, P.P. Bhattacharjee, A.H. Chokshi, Superplastic-like flow in a fine-grained equiatomic CoCrFeMnNi high-entropy alloy, *Mater. Res. Lett.* 0 (2017) 1–7.
- [44] N.G. Jones, R. Izzo, P.M. Mignanelli, K.A. Christofidou, H.J. Stone, Phase evolution in an  $\text{Al}_{0.5}\text{CrFeCoNiCu}$  high entropy alloy, *Intermetallics* 71 (2016) 43–50.
- [45] Y. Zhang, T.T. Zuo, Z. Tang, M.C. Gao, K.A. Dahmen, P.K. Liaw, Z.P. Lu, Microstructures and properties of high-entropy alloys, *Prog. Mater. Sci.* 61 (2014) 1–93.
- [46] M. Yang, X.J. Liu, H.H. Ruan, Y. Wu, H. Wang, Z.P. Lu, High thermal stability and sluggish crystallization kinetics of high-entropy bulk metallic glasses, *J. Appl. Phys.* 119 (2016) 245112.
- [47] B. Million, J. Ružičková, J. Velišek, J. Vreštal, Diffusion processes in the FeNi system, *Mater. Sci. Eng.* 50 (1981) 43–52.